CONTACT ELECTRIFICATION AND CHARGE SEPARATION IN VOLCANIC PLUMES

A Thesis
Presented to
The Academic Faculty

by

Molly Eileen Lindle

In Partial Fulfillment
of the Requirements for the Degree
M.S. in the
School of Earth and Atmospheric Sciences

Georgia Institute of Technology
May 2011

CONTACT ELECTRIFICATION AND CHARGE SEPARATION IN VOLCANIC PLUMES

Approved by:

Dr. Josef Dufek, Advisor
School of Earth and Atmospheric Science
Georgia Institute of Technology

Dr. Carol Paty
School of Earth and Atmospheric Science
Georgia Institute of Technology

Dr. Michael Bergin
School of Earth and Atmospheric Science
Georgia Institute of Technology

Date Approved: 1 April 2011

For my mother

ACKNOWLEDGEMENTS

I would like to take time to thank my research group, Dr. Josef Dufek, Mary Benage, Jenn Telling, Cindy Jackson, and Joe Estep, as well as my family, without whom I would not have been able to complete this work: my mother, Abby, my brother, Peter, and my fiancé, Benjamin Gowen. I would also like to thank Dr. Carol Paty, Dr. Mike Bergin, Chuanfei Dong, Dr. Christian Huber, Dr. Jérémy Riousset, and Tina Marstellar.

TABLE OF CONTENTS

LIST OF TABLES

LIST OF FIGURES

SUMMARY

Volcanogenic lightning has a long documented history in the scientific field, though its origins are still poorly understood. The interactions leading to electrification of ash plumes is essentially a function of the microphysics controlling and affecting ash particle collisions. This thesis presents measurements made on charged particle interactions in a fluidized bed, with large-scale applications to the phenomenon of volcanogenic lightning and charged particle dynamics in volcanic plumes. Using a fluidized bed of ash samples taken from Ecuador's Volcán Tungurahua, particles are introduced to a collisional environment, where they acquire an associated polarity. A charged copper plate is used to collect particles of a given polarity, and particle size distributions are obtained for different weight fractions of the ash. It is observed that relatively smaller particles acquire a net negative charge, while larger particles in the sample charge positively. This is a well-documented occurrence with perfectly spherical, chemically identical samples, but this work represents one of the first applications of the principle to volcanic ash. Image analysis is preformed to determine the size distribution associated with specific polarities, and the associated minimum charge on each particle is calculated based on the plate collection height and particle size. We also present results that demonstrate the relationship between particle collisions and the amount of charge exchanged. Using techniques developed to examine the collision rate within a flow, combined with the charging rates determined from this experiment, we determine a maximum charge exchange rate of 1.28±0.23 electrons transferred per collision.

CHAPTER 1

INTRODUCTION

Introduction

Volcanogenic lightning has a long documented history in the scientific field (*Hoblitt 1994, James et al. 2008, Lamoreaux 1995 Chakraborty 2009),* though its origins are still poorly understood. The phenomenon leading to electrification of ash plumes is at its core a problem of the microphysics of ash particle collisions. Erupting magma is fragmented during its exit from a volcanic conduit, and this fragmented material forms the bulk of the solid portion of the eruption column. The gaseous part of the column is comprised of atmospheric gas entrained by the turbulent column, and erupted volatiles, primarily water and carbon dioxide, along with smaller amounts of sulfur dioxide (*James et al. 2008*). Due to the turbulent nature of the column, the high energy of the jet flow, and the high particle concentration, collisions are frequent and occur throughout the column's depth. These collisions can lead to triboelectric charging, which is a function of the static friction associated with the colliding particles (*Textor et al. 2006*). It has been observed in collisional flows of spherical particles, that as particles collide, they acquire a charge, with larger particles holding a net positive charge, and smaller particles holding a net negative one (*Forward et al. 2009*). Application of this theory to volcanic ash particles leads to the idea that, as smaller ash particles naturally drift upward, this creates a charge differentiation through which small-scale (1m or less) lightning can arc (*James et al. 2008*). The mechanism behind the size-charge correlation is poorly understood, though theories exist to try to explain the phenomenon (*Lowell 1986*). These theories will be discussed in detail in later chapters. The purpose of the work presented in this thesis is to explore, using a fluidized bed of ash particles, if there is a distinct charge-to-size relationship that exists as a result of particle collisions within a fluidized bed of volcanic ash, as well as to shed light on particle charge exchange via these triboelectric interactions.

Previous Studies in Particle Charging

Particle Charging in Laboratory Experiments

Many experiments have been conducted to demonstrate the correlation between size and charge in collisional situations (though this work is one of the first to apply the techniques with ash, as opposed to chemically identical, monodisperse spheres). One of the experiments most relevant to this work was conducted by *Forward et al.* in 2009. This work used three separate monodisperse sample size distributions of spherical soda lime glass with mean particle diameters of D = 78 μm (σ = 13 μm), D = 137 μm (σ = 22 μm) and D = 321 μm (σ = 22 μm). Bimodal samples were created by mixing samples from each batch at different mass fractions. These samples were fluidized within a small chamber for roughly two hours. After the duration, a plate connected to a high voltage source (positive or negative) was placed above the bed to collect particles of a specific charge polarity. After representative amounts of charged particles were collected, the particle size distributions (PSD's) were found using an optical microscope, along with the mass of each polarized sample.

The results of this experiment showed that when mass fractions of large particles to the total sample were 0.70-0.80, there was a clear tendency of larger particles to charge positively, and smaller particles negatively. When the mass fraction was close to 0.5, smaller particles charged both positively and negatively; likewise, when the mass fraction was close or equal to 1.0, larger particles tended to charge with either polarity. This indicated that the *relative* size distribution of the particles in the sample was the important factor in determining how particles will charge; this was further substantiated when different bimodal samples were used to obtain representative particle size distributions. In every case, the relative sizes of the particles determined the resultant polarity.

Electric Fields in Volcanic Plumes

Several papers have detailed the effect of electric fields on charged particle interactions, especially in thunderstorms, dust devils, and convecting ash plumes (*Dwyer et al. 2009, Farrell et al. 2003, Rasmussen et al. 2009)*. While background electric fields have been observed to be in place before eruptions occur, the exact cause of these electric fields is not yet known; it is true, however that the charged particle interactions themselves can lead to the generation of such electric fields. In these cases the occurrence of lightning acts to discharge across the electric field and bring the system back to equilibrium (*Riousset et al. 2007*). While the precise role that electric fields play in volcanic lightning is not explicitly understood, the existence of electric fields in convecting ash plumes has been well-documented and modeled (*Rasmussen et al. 2009*).

Electric Fields in Laboratory Charging Experiments

Further work in the area of collisional dynamics treated the interaction of particles in a fluidized bed with an applied background electric field (*Pahtz et al. 2010*). The model presented in this work treated monodisperse, equally-sized beads interacting in a fluidized bed in the presence of an electric field. The results from this model, as well as physical experiments to test it, demonstrated another way positive charge can accumulate at the base of a flow and negative charge at the top. This experiment did not address the issue of size distributions, but rather how the electric field itself can lead to differential charging in colliding ash particles by repolarizing particles that become neutral upon contact (a collision). This, according to this paper, leads to a net accumulation of negative charge on the top of a particle, and a net accumulation of positive charge on the bottom of the particle. While this model presented viable methods for examining charge exchange in particle collisions, the associations between particle size and charge were not addressed and still remain elusive to the scientific community.

Electron Transfer via Collisions

Theories do exist as to why small particles accumulate negative charge and large particles positive charge; the most accepted theory to date entails the transfer of electrons in an excited state on one particle to the ground state on another particle as a result of a collision (*Lowell et al. 1986*). According to this theory, particles can have surface electrons trapped in excited states (since electron states are spatially localized on ash particles) that can only move to the ground state on another particle via collision, rather than emission. The larger a particle is, the more excited electrons it can have on its surface. As collisions occur within a fluidized region, the net number of electrons in excited states decreases as the number of electrons in ground states increases, indicating a movement from one state to the other, via these collisions (*Lacks and Levandovsky 2007, Lacks et al. 2008*). *Duff et al. 2008* demonstrate in their paper that as the number of electrons in high-energy states decreases over time, the number of electrons in low-energy states increases proportionally. It is worth noting here that these particles are treated as perfect spheres, not rough ash (or any other small jagged particulate).

In the model presented in *Lacks and Levandovsky* 2007, particles are represented in two size distributions, one larger, one smaller. All particles are initially assumed to have identical surface densities of trapped electrons, proportional to the surface area and number fractions of each particle in the sample. At the same time, all particles are assumed to be initially neutral. In the running of the model, each particle is allowed to collide with large and small particles, each time transferring a high-energy electron to a lower state on the other particle, and receiving a low-state electron on its own surface from the collision. Collision fractions are determined for the small and large size distributions; these are based on the radii of both distributions, and the number fractions of the large and small particles. These collision fractions are then used to calculate the average charge on the large and small particles. The results of this model show that collisions between particles with high-energy state surface electrons can lead to a net negative charge on smaller particles and a net positive charge on larger ones. (*Lacks and Levandovsky 2007*).

Motivation for This Work

Volcanic Lightning

Reports of volcanic lightning go as far back as the cataclysmic eruption of Santorini in 1450 B.C.E. (*Lamoreaux 1995*); volcanic lightning has come into some notice in the last few decades with the eruptions of Mt. St. Helens in 1980, Mt. Redoubt in Alaska in 1990 (*Hoblitt 1994*), and Mt. Pinatubo in 1992 and Chaitén Volcano in Chile in 2008 (*Chakraborty 2009*). Volcanic lightning can occur when lava or pyroclastic flows encounter water, leading to phreatic explosions and, often, charging associated with the water molecules (*Anderson et al. 1965*). A common cause of volcanogenic lightning is the differential charging of individual ash particles within the plume, which can arc over small vertical distances (*James et al. 2008*). While lightning has come to be regularly associated with large, Plinian eruptions, the exact cause of this differential charging that leads to it remains elusive to the geophysical sciences. While the Chaitén eruption of 2008 provided stark evidence for the occurrence of volcanogenic lightning, along with sensational photographs of the event, it did not supply a large amount of viable data to help scientists understand why and exactly how volcanogenic lightning occurs.

Figure 1: Image from the 2008 eruption of Chaitén Volcano showing multiple lightning strikes in and around the ash plume (Courtesy C. Gutierrez/UPI, http://nasadaacs.eos.nasa.gov/articles/2009/2009_volcanoes.html)

Direct measurements within the plume are virtually impossible, given the highly dangerous nature of large-scale eruptive columns. Measurements made at the 1990 eruption of Mt. Redoubt, using a commercially-available Lightning Detection System operated by the Alaska Fire Service, yielded a more substantial base of results, showing a high number of volcanic strikes; scientists observing the eruption were able to determine the position and charge of these occurrences (*Hoblitt 1994*). This LDS used field sensors connected to dedicated phone lines to detect broadband radio signals from lightning strikes within the eruption and ensuing pyroclastic flows. Measurements made at Sakurajima volcano in Japan showed distinct perturbations of the background electric field and atmospheric electric potential gradient as a result of activity at the volcano (*James et al. 1998*).

Summary of Project Goals

This work primarily provides for the association of physical parameters to the phenomenon of collisional charge exchange, as well as verification of a charge-to-size correlation in collisional ash settings. *Lowell et al. 1986, Lacks et al. 2006, Lacks and Duff 2008,* and *Duff et al. 2008* demonstrated in their papers that electrons can move from a high-energy state on one particle to a low energy state on *another* particle following a collision; the goal of the work presented here is to perform laboratory work to assess the rates at which charging on a macroscale due to numerous collisions occurs. Since charge can be assumed to transfer in a given collision, the charge exchanged, or, as would seem to be more useful, the number of electrons transferred for a given collision, can be determined from the collision rates of the flow and the average charge on a collected particle. In the chapters following the project will be largely presented as an experimental work; though numerical analysis was performed to aid the experiment, it is not presented separately, as each numerical step was taken in order to better understand the experimental data. This laboratory work utilizes three methods: first, the determination of a polarity-to-size ratio for volcanic ash in a fluidized bed; second, the determination of collision rates in a fluidized ash bed using the method of *Telling and Dufek M.S. Thesis, 2010;* this method utilizes high-speed camera images and a 2-dimensional slice of a fluidized bed. The third method employed in the lab involves the

collection of fluidized, and thus triboelectrically charged, particles via a charged copper plate. The minimum charge on each particle collected is determined, based on its size and collection height (described in more detail in the following chapters). Combining the data from the second and third methods yields an upper bound on the minimum charge per collision in this fluidization environment.

CHAPTER 2

EXPERIMENTAL METHODOLOGY

Experimental Apparatus and Setup

To begin the experiment, ash collected from one of our field sites (Ecuador's Volcán Tungurahua) is sieved into separate size bins, <90 μm, 90-106 μm, 106-125 μm, 125-212 μm, 212-250 μm, and >250 μm. The >250 μm and <90 μm samples are not used here, due to a higher potential variability in particle sizes. For this experiment we choose 90-106 μm and 125-212 μm to represent the small and large particles, respectively, so that D_L = 125 μm-212 μm, and D_S = 90-106 μm. The weight fraction of a given sample is

$$w_L = \frac{m_L}{m_L + m_S} \tag{1}$$

where m_L is the mass of the larger sample and m_S is the mass of the smaller sample. In order to determine a weight fraction to use in our experiments, we examine the results of *Forward et al. 2009*. The most likely mass fractions with which to see the strongest example of differential charging fell between w_L = 0.70 and w_L = 0.80 in the *Forward et al. 2009* experiments; therefore we are using a mass fraction of 0.75 for our trials here. As a check on this decision, other mass fractions ranging from 0.70 to 0.85 were also used, with 0.75 showing the highest tendency to lead to differential charging for ash. Future iterations of this experiment will detail the effect of higher or lower mass fractions on the data sets collected. The experimental setup used is shown in Figure 2.

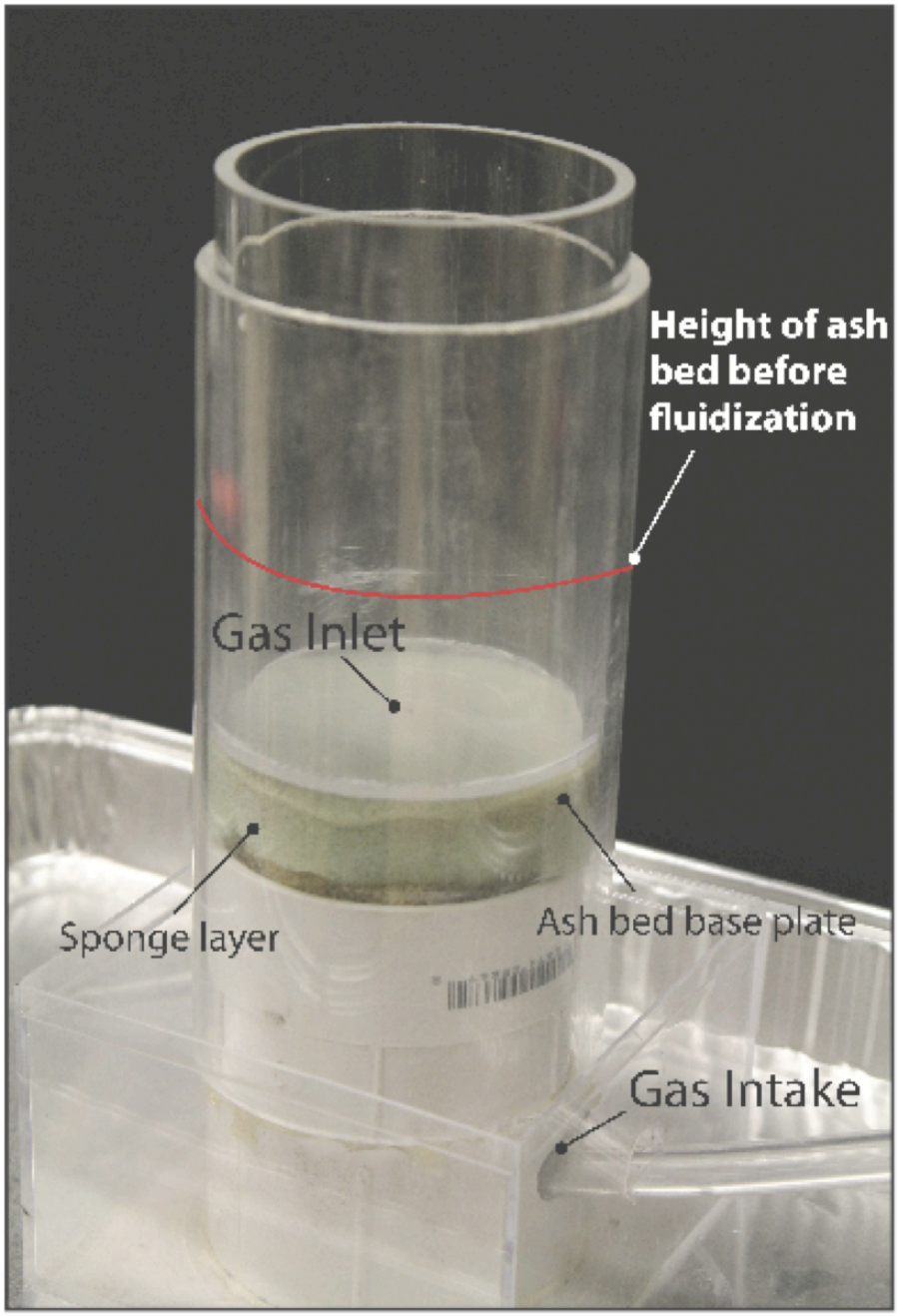

Figure 2: Experimental apparatus used for conducting charge exchange and collection height trials.

Two concentric plexiglass cylinders sit above a foam insert through which gas can be run. Above the smaller cylinder, which sits within the larger, taller cylinder, and above the foam insert is a clear plastic cover with an inlet hole roughly 2 mm in diameter, so that incoming gas can be directed upward into the ash samples. Ash is placed above the plate, in a bed of approximately 8cm height. The plexiglass tubes are covered and dry

nitrogen is run through the system at 100-140 Pa (the thickness of the bed prevents using lower pressures, but ensures that any up-thrown particles are returned into the flow for more collisional events, as observed by *Forward et al. 2009*).

Collisional Charging

The two size samples are combined into a weight fraction of 0.75, using plexiglass boxes to ensure that no ash is lost in the combination process. The sample is then transferred via this box to the experimental apparatus shown in Figure 2. The height of this bed, prior to collection, is measured with a lab ruler. Sample boxes are prepared to house the collected particles once they have been imaged; these boxes are placed on a scale and tared. The nitrogen tank is then connected to the experimental apparatus, and dry nitrogen is pumped in below the plexiglass tubes. The bed of ash is allowed to fluidize for 15 minutes, after which the nitrogen supply is removed and, as can be seen in Figure 3, a charged plate is suspended over the bed. This plate is connected to a rotating rod that can be raised and lowered as needed. The length of this rod is measured, in order to determine the plate height above the bed for collection; prior to collection the resting height of the bed is measured, to compare to the rod length. The copper plate is coated with a thin layer of parafilm to prevent particles from moving to the plate and discharging before they can be collected.

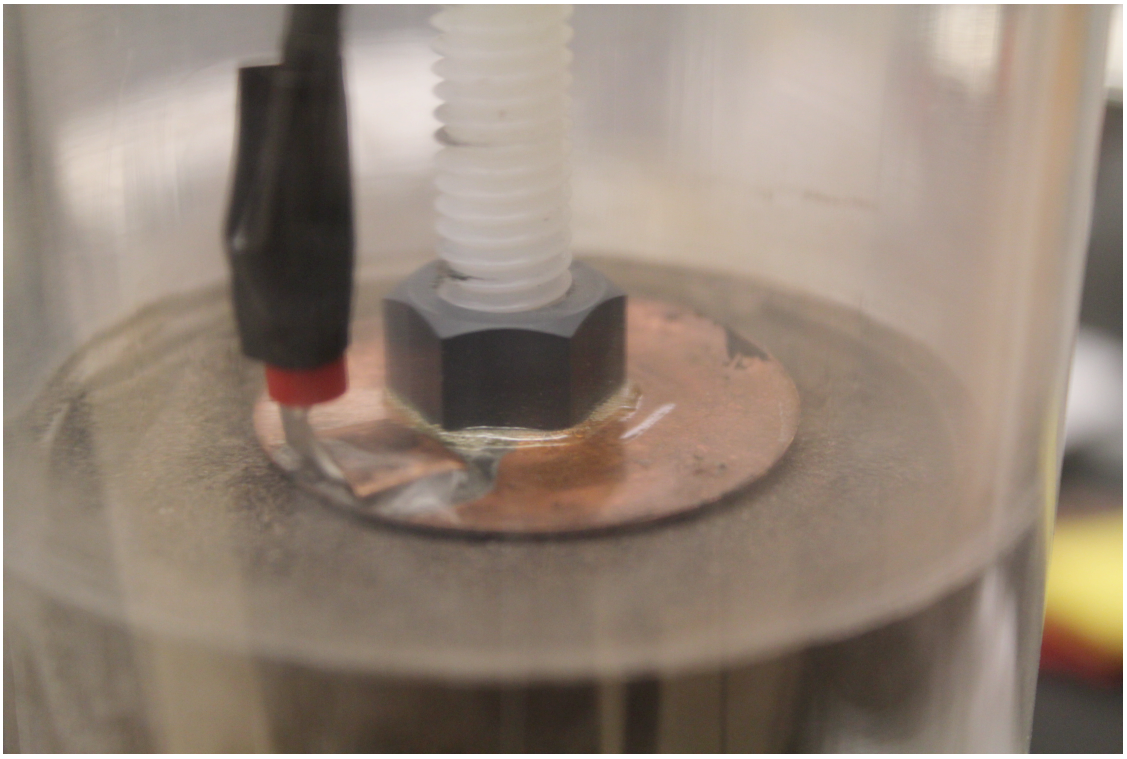

Figure 3: Collection process using charged copper plate and formerly fluidized ash bed. Plate is connected to a rotating rod that lifts or lowers the plate smoothly above the bed.

Once the plate is in place above the bed, it is connected to a ±5 kV source that ranges at any given time between ±4.9 and ±5.1 kV. Multiple height trials are run in which the plate is raised or lowered from 2-5mm above the bed. The plate collects above the bed for 60 seconds, after which the particles that have been attracted to the plate are transferred to the sample box resting on the tared scale. The plate polarity is then switched and it is placed back above the bed for another 60 seconds. A second sample box is labeled and placed on the scale to receive the next set of collected particles. This process is repeated twice more, for a total of three collections per fluidization for each polarity. Each time the bed height is re-measured to ensure the least introduction of error from this effect. Once these six collections are complete, the particles within the sample boxes are transferred from the box to pre-made imaging paper for photo processing. A DSLR camera with a macro lens attachment is used to take high-resolution photo images of the particles on the grid paper, which contains a length scale for later conversion of particle sizes into actual units (see Figure 4).

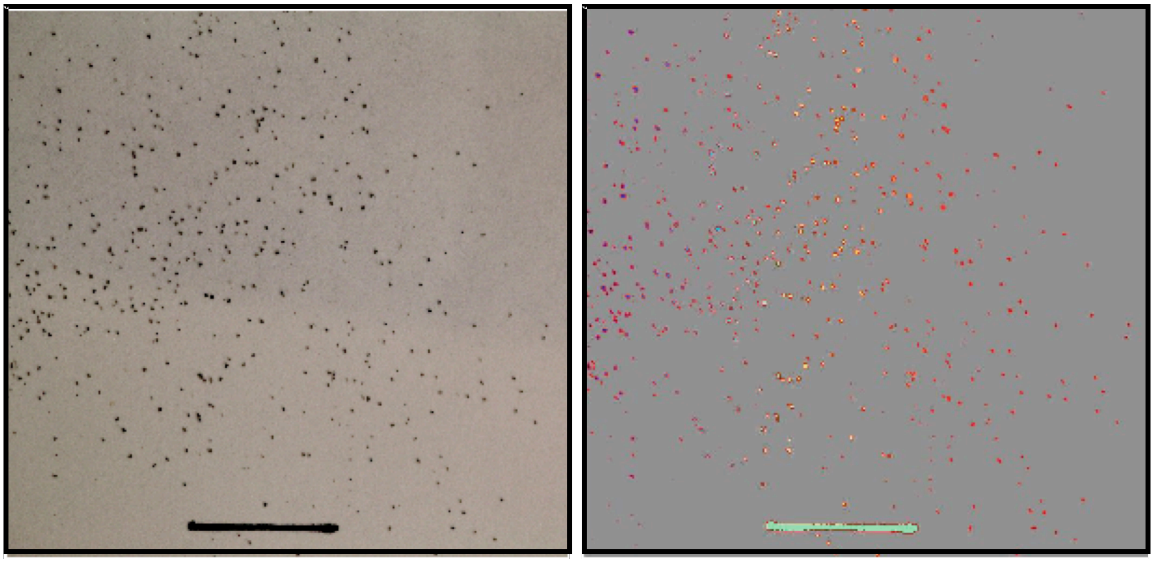

Figure 4: Imaging analysis. Left side shows an imaging grid prior to size analysis; line at the bottom is inserted for scale (1 cm). Right side shows same image post-analysis. The code detects and sizes each particle in px, and uses the scale conversion to convert to μm.

Height Trials

One of the potential areas for error or erroneous data collection with this work is the type/number of particles collected for a given collection height of the copper plate. Placing the plate too close to the bed allows for the Coulomb force from the plate to be significantly larger than the gravitational force felt by a particle, and too many particles are collected for reliable imaging; the data is essentially 'swamped' with particles. Placing the plate too far away from the bed allows only for collection of the very smallest particles, which are difficult to image and not representative of the actual charging dynamics taking place. To remove potential bias from this effect, trials are run from 1-6 mm, in increments of 1mm, to determine the optimum height for collection; trials run at 6 mm height were removed from the data set because virtually no particles were collected at this height. Trials run at each collection height follow the method outlined in the previous section.

Imaging

The particles are transferred from the plate to pre-made imaging sheets for image processing. This involves using a macro lens DSLR camera to take multiple photos of the sheets. Each box on each sheet contains a tick mark that represents 1 cm. This factor is used in converting from pixel data to real units. The images taken, one of each square on the imaging sheet, are processed using a MATLAB code originally written to determine the 'roundness' of a given particle (*Manga et al., 2010*). The code uses a principle of black-on-white (or vice versa) to detect particles in an image; it then determines the number of pixels comprising the area of the particle, its major axis, and its minor axis. These values are then used to determine the average radius of each detected particle in the image. The 1 cm tick marks are then used as references to convert pixel data into μm. A sample image of the photo pre-processing and post-processing is provided in Figure 4. This process is performed individually for each collection event, separately for the negatively and positively charged particles. This data is then used to generate a combined histogram for each height trial (see Figures 6-10).

Collision Rate Experiments

The second segment of this experiment involved determining the rate of collision within the ash bed. This was done using a method developed by *Telling and Dufek M.S. Thesis, 2010;* the ash bed is placed below a 532 nm NdYag laser sheet of thickness 250 μm, and allowed to fluidize. A high-speed camera is placed in front of the illuminated bed; once the bed has been fluidizing for approximately two minutes, the high-speed camera is activated and images are taken for approximately 5 minutes. From these images a representative sample is clipped (this is done by visually assessing the 'movie' generated from the high speed images and clipping segments from the set; see Figure 5 for images clipped from one such segment); the images are run through processing software developed by *Telling and Dufek M.S. Thesis, 2010,* using Particle Image Velocimetry (PIV) techniques.

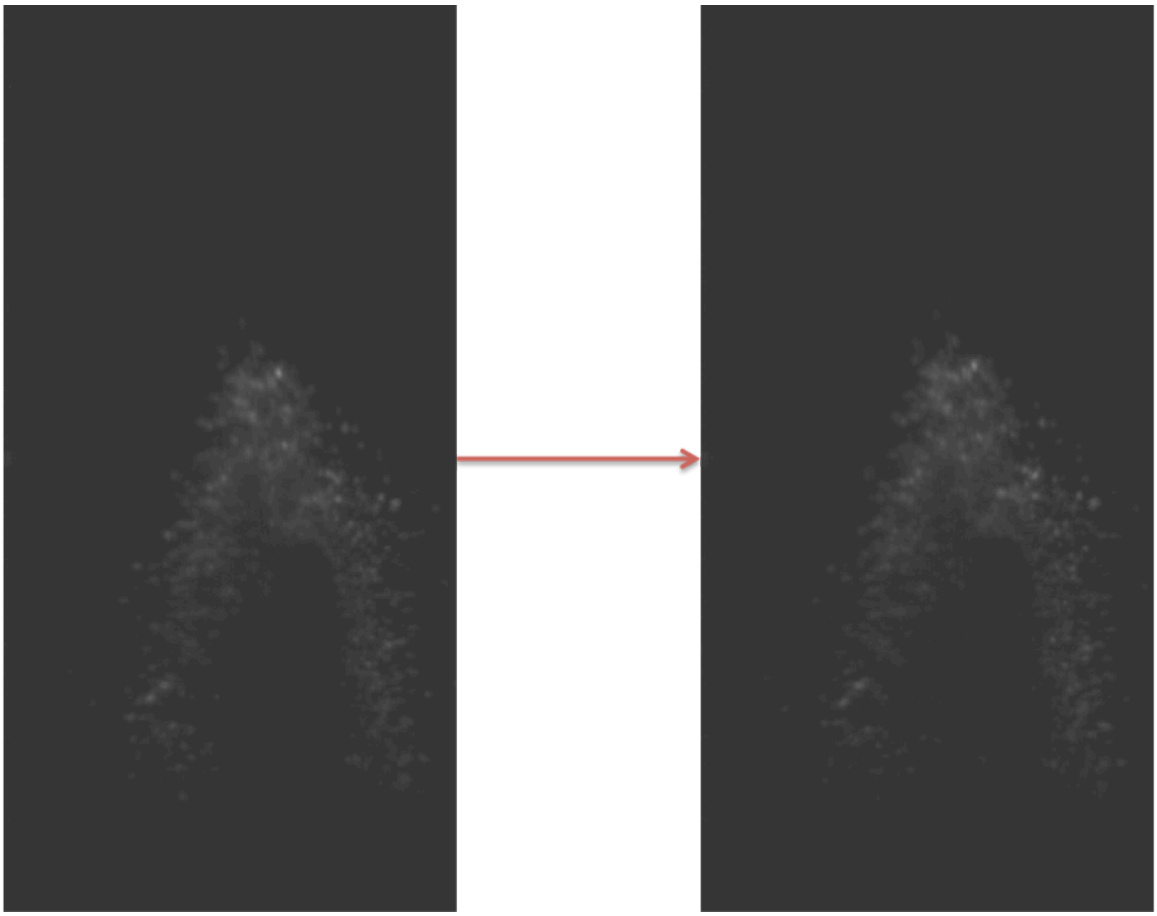

Figure 5: Two consecutive images taken from a representative run of the PIV software. The software detects collisions by analyzing particle locations in consecutive images (see *Telling and Dufek M.S. Thesis, Georgia Inst. Technology, 2001*)

The results from this tracking software yield a collision rate in units of collisions per second per volume, since the images are taken of what is essentially a very thin three-dimensional sheet. A conversion factor is introduced to determine the overall collision rate, called C, where C is

$$C = \frac{h_f \cdot w_f \cdot t_f}{h_s \cdot w_s \cdot t_s} \tag{2}$$

Here, h_s, w_s, and t_s, represent the height, width, and thickness of the laser sheet (the height and width are the image height and width determined prior to image processing). The h_f, w_f, and t_f represent the approximate height, width, and thickness of the flow as determined from a representative sample of images. This factor allows for the determination of the total collision rate within the flow.

Numerical Analysis

In order to determine the minimum charge present on each particle in order for collection to occur (i.e. for the Coulomb force between the particle and plate to be larger than the gravitational force on the particle), we utilize the equation for the electric field of a charged plate as introduced by *Parker 2002* to find the charge on a particle for a given collection height:

$$Q_p = \frac{\frac{4}{3}\pi R_p^{\,3}\rho g}{\frac{V}{2}\left[\frac{r_l^{\,2}}{(r_l^{\,2}+H^2)^{\frac{3}{2}}}\right]} \tag{3}$$

This gives a minimum constraint on the particle charge. Here, V is the voltage applied to the plate (V), r_l is the plate radius (m), H is the plate height above the bed (m), R_P is the particle radius (m), ρ is the density of the ash particle (kg/m^3), and g is the gravitational acceleration (N/kg). Here we assume the ash to have an average density of 2400±50 kg/m^3, and the plate diameter is measured to be 3±0.05 cm. The voltage applied is ±5±0.1 kV, and gravity is assumed to be 9.8 N/kg. Error for the density is assumed from the range of densities presented in *Shipley and Sarna-Wojcicki 1982* for volcanic ash. Error in the plate is determined from the error in caliper measurements made, and the error in the voltage applied is determined from fluctuations in the voltage source over the course of the experiments.

CHAPTER 3

RESULTS

Collisional Charging

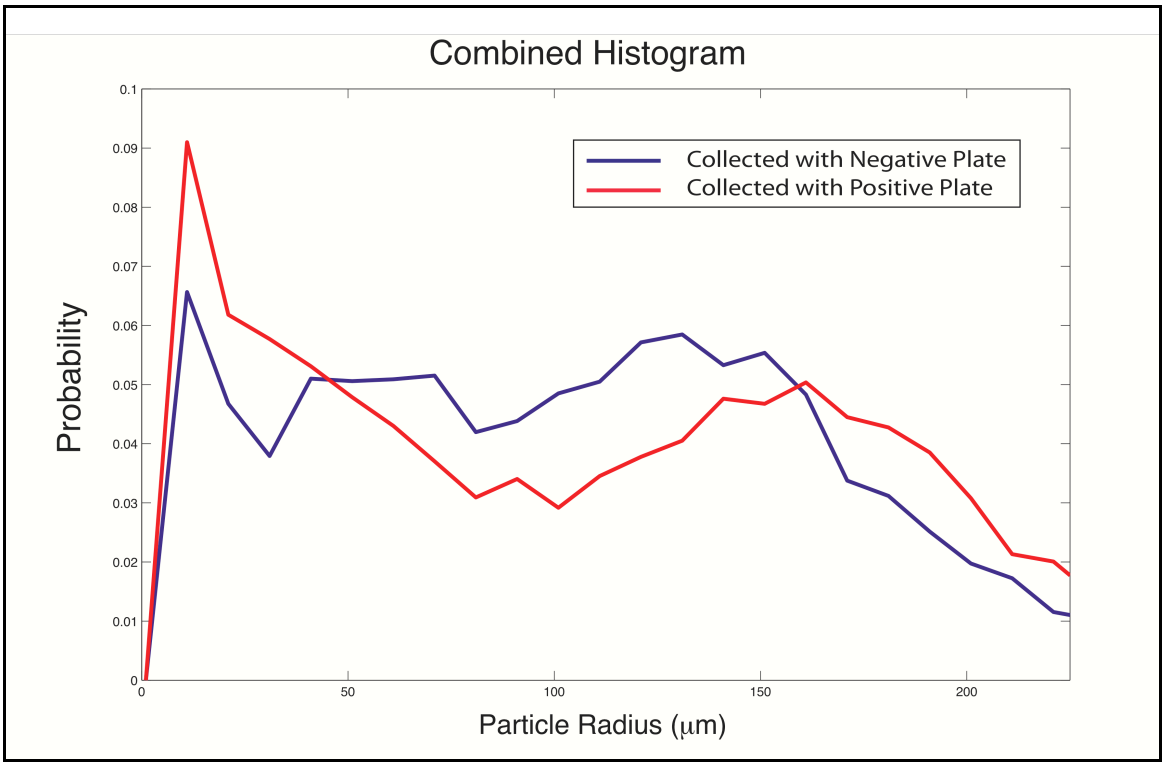

Figure 6: Particle Size Distribution (PSD) for entire data sets (combined data from each height trial). Note the peaks in smaller radii for negatively charged particles, and peaks in larger radii for positively charged particles

This histogram shows results for fluidization and collection events performed to determine whether or not there exists a relationship between a charged particle's polarity and its relative size within the sample. The x-axis shows the particle radius in μm, while the y-axis shows the probability as it relates to the total number of particles collected following fluidization. The data in this plot is representative of each of the collection events performed in the height trials; that is to say, this plot represents data collected at heights ranging from 2-5 mm. Particles collected with a negatively charged plate are represented with a blue line, while particles collected with a negatively charge plate are

represented with a red line; this is true of all further histograms presented here. In this particle size distribution it can be seen that smaller particles are collected in greater numbers by the positively charged plate, while larger particles are collected in greater numbers by the negatively charged plate.

Height Trials

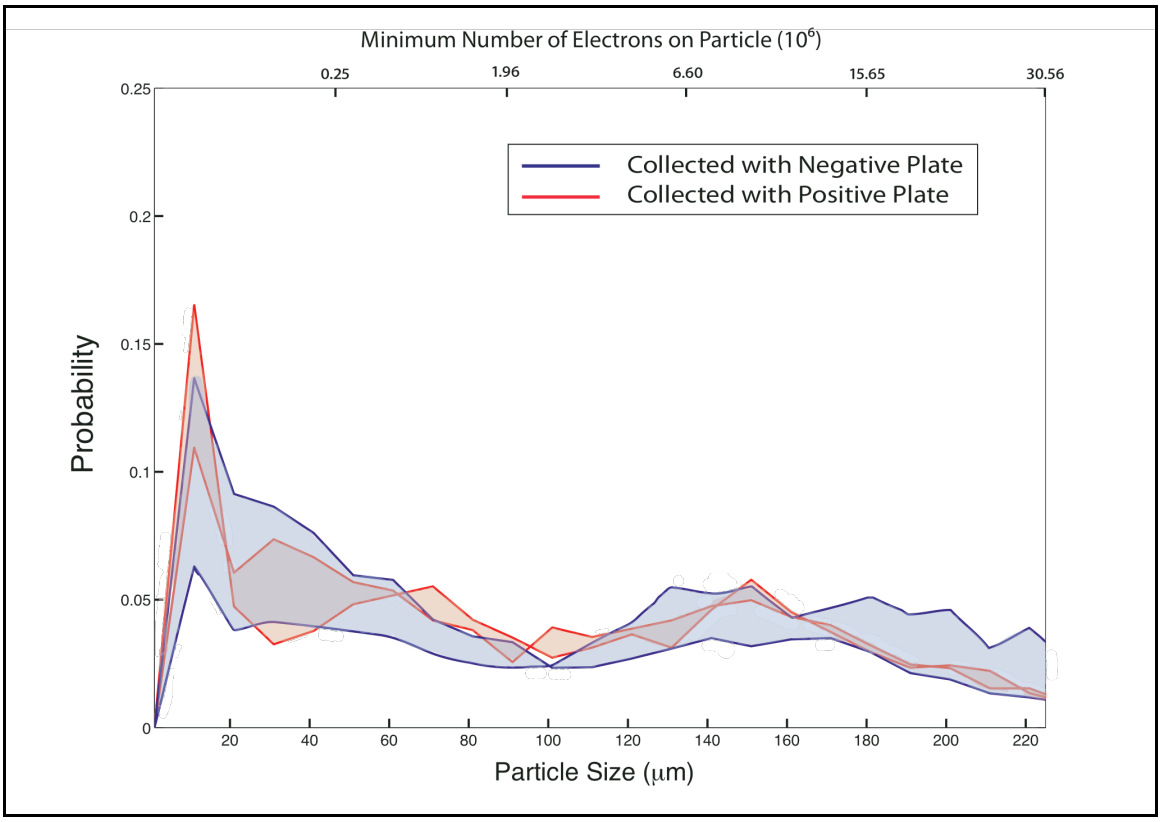

Figure 7: PSD for a collection height of 2 mm. The shaded regions in the PSD represent the probability for a given particle height based on overall number density, for multiple trials run using this collection height. Note the addition of a third axis, representing the minimum number of surface electrons (in millions) on a particle of a given size required for collection. Note that there are primarily only smaller particles being collected here, with distinct peaks present in both the small and large particle ranges.

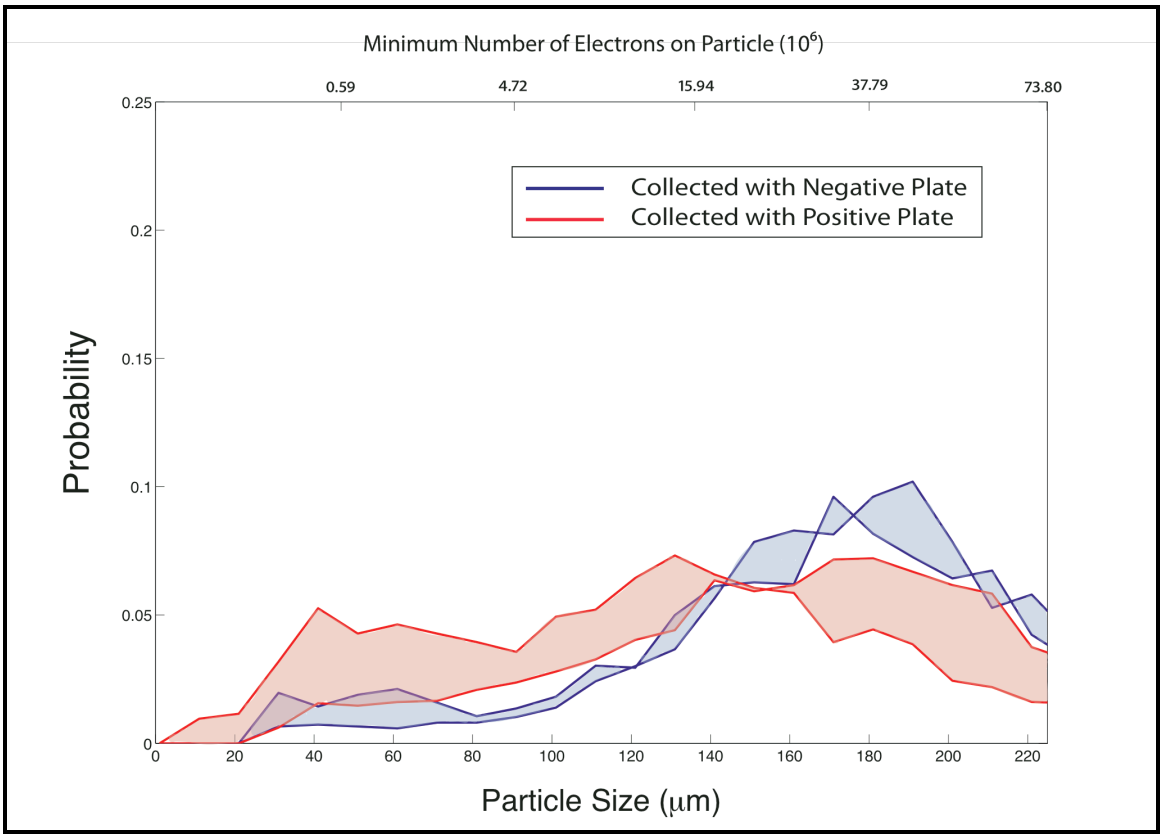

Figure 8: PSD for a collection height of 3 mm. Shaded regions represent multiple trials run at this height. In this case, distinct peaks exist in the larger particle range for those particles collected with the negative plate (i.e. positively charged particles), while significant peaks exist in the smaller particle range for those particles collected with the positive plate (i.e. negatively charged particles).

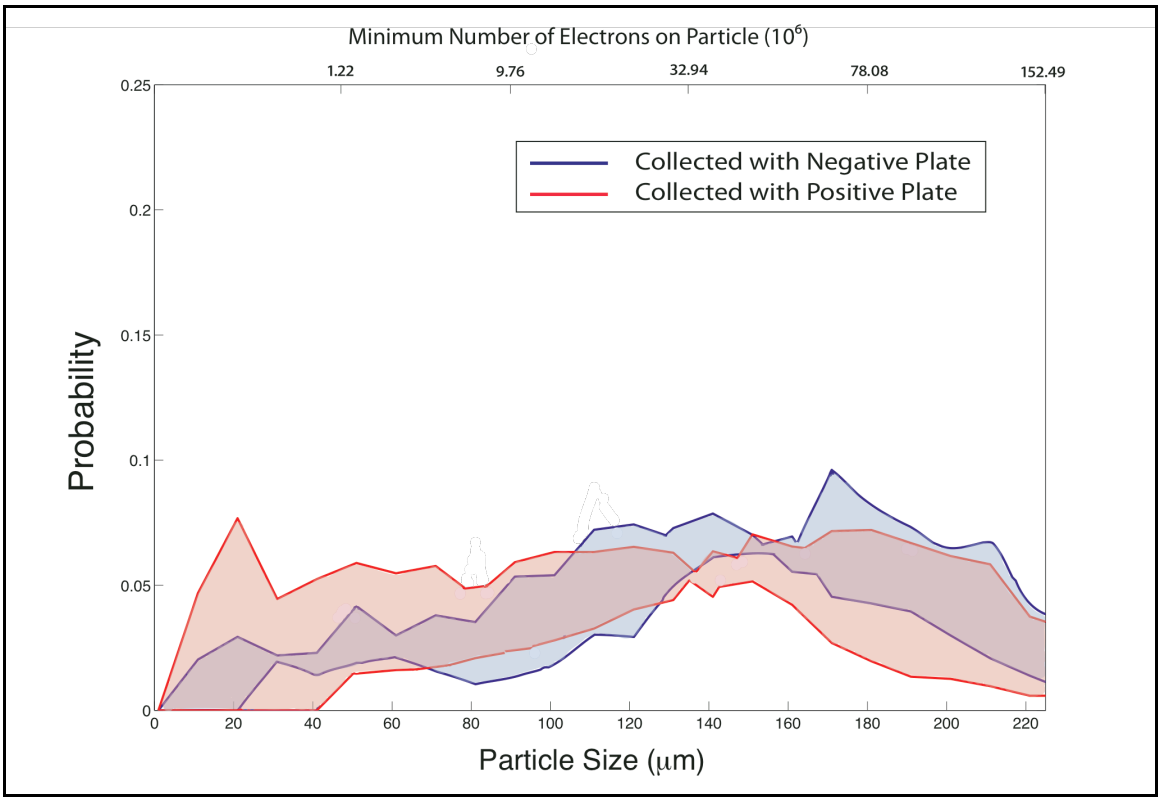

Figure 9: PSD for a collection height of 4 mm. Shaded regions represent range of data collected from multiple runs conducted at this height. The size-to-charge associated peaks are clearer here than before, with peaks in the larger size range corresponding to positively charged particles, and peaks in the smaller particle size range corresponding to negatively charged particles.

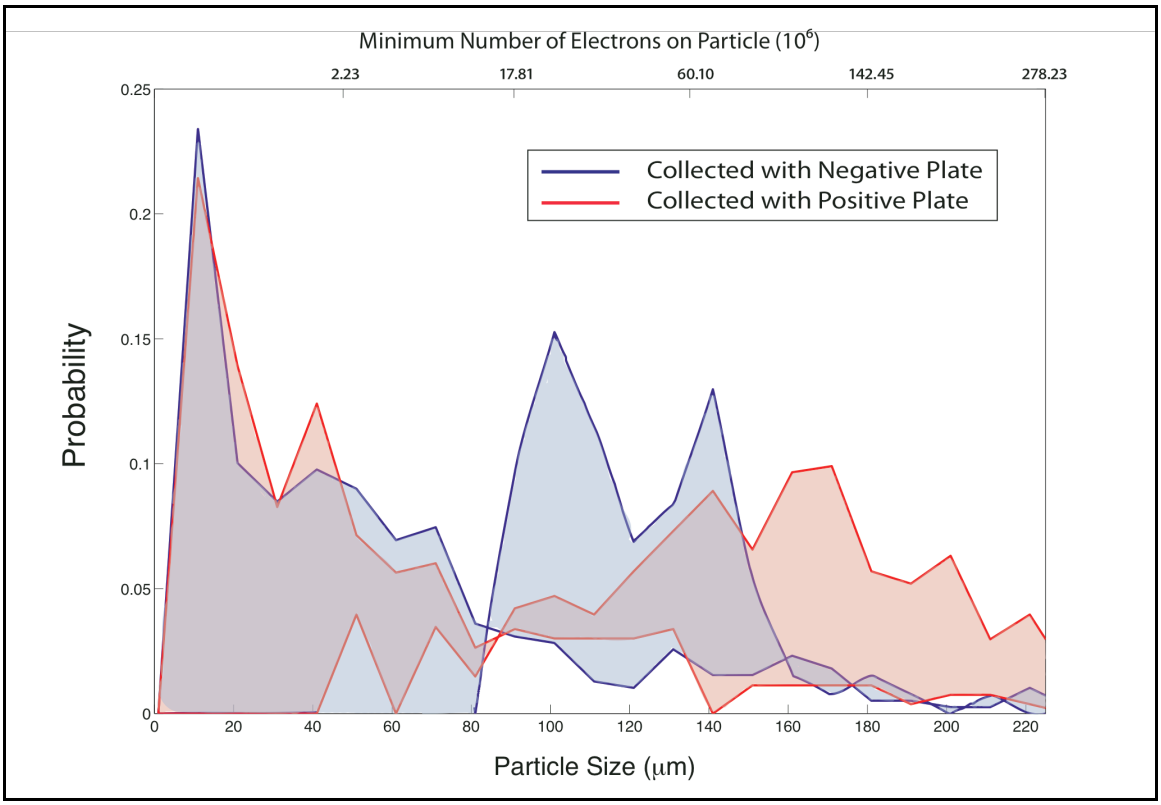

Figure 10: PSD for a collection height of 5 mm. Shading represents the range of data collected using multiple trials at this collection height. In this case the majority of particles collected were small, due to the increased collection height. There are two distinct peaks in the 80-150μm size range for the positively charged particles, but this data is not as strongly weighted in the overall set due to its being noticeably inconsistent with the rest of the data.

Each histogram shows a correlation between the polarity of the particles collected and their size; in general, smaller particles are collected in greater numbers by the positive plate, and larger particles are collected in greater quantity by the negative plate. In Figure 10 it can be seen that only smaller particles are collected, due to the greater collection distance than the other height trials. Smaller particles showed a tendency to charge both negatively and positively here, but due to the biasing of collection from the increased collection height, this is not treated as an accurate representation of the charging dynamics occurring within the flow.

Collision Rate Experiments

Table 1: Collision rate as determined using the PIV techniques of *Telling and Dufek M.S. Thesis, 2010*. Each collision rate is shown with its corresponding number of collisions detected by the program. The overall rate is a weighted average based on the number of collisions detected in that run.

Collision Rate (Collisions/s)	# Collisions Detected
17.5	1
18.75	1
140	21
248	46
292	54
306	7
742	98
872	133
937	164
1640	481

Using Particle Image Velocimetry methods (PIV), high-speed camera images such as those shown in Figure 5 were analyzed to determine collision rates. The 2-dimensional collision rate for the flow used in this experiment was determined to be 1157 collisions/s, with an error of ±7 collisions/s. The error in this rate was assessed by using two separate methods to determine the average collision rate; one method determined an average weighted collision rate, based on the number of collisions detected by the program. The other method determined the collision rate based on the overall average rate. In each case the values were within 7 collisions/s of one another, and so this was taken to be the error. This represents the 2-dimensional value for the collision rate, and so equation (2) is used to determine the 3-dimensional value. The scale of the images in Figure 5 is known from measurements made during the experiments; the height of the image is 37.5 cm, and the width is 17.5 cm. The thickness of the laser sheet is 250 μm. From these measurements, we were able to measure the average height of the flow to be 21.75 cm, and the width (which is assumed to be equal to the thickness, as the flow is generally symmetric) was found to be 8.29 cm. The value of C was therefore determined to be: 92.05. This gives a 3-dimensional collision rate of 1.06e5 collisions/s.

Charging Analysis

Using equation (3), the minimum required charge on a collected particle was determined for the size ranges presented in the particle size distributions. Incorporating the errors discussed in Chapter 2, the error on each charge is 6.84e-13 C. Incorporating the time over which the particles were permitted to fluidize (900±30 s), allowed for the charging rate to be determined for any given particle. In order to obtain a maximum constraint on the possible charging rate, the average maximum charge from the height trials was used as the charging value. It was determined to be 1.41±0.26e-14 C/s. This error is determined by finding the maximum and minimum possible values for the charging rate based on the maximum and minimum possible charges and fluidization times. Using this value, and the collision rate as determined above, we determine a maximum bound on the charge exchange per collision to be 1.28(±0.23)e-19 C/collision, or, perhaps more intuitively, roughly one electron per collision (see Chapter 4: Discussion, for more information on the error analysis).

CHAPTER 4

DISCUSSION

Collisional Dynamics

The first objective of this experiment was to determine whether or not the documented phenomenon of differential size-based charging is present in ash collisions. Based on Figures 6-10 above, it can be seen that a relationship is indeed present, though it is less distinct than is seen in monodisperse, chemically identical samples. A few explanations exist for the range of particle sizes collected. In this experiment the two mass fractions combines did not represent particles of one single size; rather, as stated above, the smaller set contained ash of radius 90-106 μm, and the larger set comprised particles of radius 125-212 μm. This fact lends to a larger spread in the number of larger particles which end up charging negatively, and vise versa, since the 'large set' in fact contains it's own range of small to large particles. The particles in this experiment are also rough, asymmetrical, and not necessarily chemically identical. These factors can affect the collisional dynamics at play in the system; asymmetrical particles, despite having a 'radius,' can have more (or less) surface for interaction than a spherical particle of the same diameter. Reactions can occur between particles of certain chemistries, and rough particles are more likely to aggregate (*Textor et al. 2006*). Even with the spread of sizes on collected particles, it can be seen that, for almost all collection heights (5 mm being the exception), more particles in the <100 μm range were collected with a positive plate (and were thus negatively charged); likewise, more particles in the >100 μm range were collected with the negatively charged plate (positively charged particles). While the goal of this experiment was not to investigate the exact reason for this correlation, literature and modeling on the subject exists (e.g. *Lacks et al. 2006, etc.*)

Height Trials

Particle collection trials were run through a range of sizes for this experiment, in order to discern the effect, if any, collection height would have on the particle size

distributions. As can be seen from the figures presented above, a distinct relationship exists between the PSDs and the collection height; for very low heights (2-3 mm), larger particles are collected in higher numbers than for higher collection heights. For a height of 5mm, only small particles were collected, as the gravitational force acting on the large particles here was able to overwhelm the Coulomb force between the charged particles and the charged plate.

The cumulative measurements shown in Figure 6 best reflect the net grain size distribution over all of the collection heights. A logical future direction for this research to take is to determine the number of particles of a given size that require a set minimum charge for collection. The charge-to-size relationship could then be determined for the experimental scenario presented here.

Imaging Process

The 1 cm-length strip in each grid enabled a more accurate calculation of the actual radii of each particle. The radii were calculated by determining the area of the given particle, and assuming a spherical shape to back out the specific dimensions. The long or short axis lengths were not used, because, given the unpredictable shapes of the ash, these could give very inaccurate radii. The only problem introduced by the imaging process was the possibility of overlapping particles in the images; since the code used converts the image to 'black on white' before processing, any overlapping particles registered as one single, larger, particle. In order to reduce this effect, first and foremost the particles were transferred to the grids carefully, and examined for overlaps. Any such instances that made it through to the image processing were filtered out, as the radii were unrealistic compared to the range of particle sizes present in the samples.

Charge Calculations and Error Propagation

It is worth noting here that the charge calculated in this instance represents the minimum charge that must be on the particle for it to be collected by the plate at the given height; the particle could in fact have more charge on the surface. It is also worth noting that the charge plotted on these graphs represents the magnitude of the charge, and

not the polarity. The magnitude of the minimum 'collection' charge will be the same for a positive or negative particle. For each of the PSDs presented in Chapter 3, the maximum charge possible for that height configuration was averaged with the others to determine the average maximum bound on the minimum charge necessary for collection that was used in the calculations above. This factor, as well as those discussed in previous chapters, introduces measurable errors that could be incorporated into the final charge exchange value. One assumption had to be made, however, to even allow for the calculations; we assumed that all of the charging occurred evenly over the 900 s the bed was allowed to fluidize; it is possible that the charging occurred over much smaller timescales. In order to investigate this effect, we determined the charging rate, using our calculated average maximum charge, as a function of the fluidization time. This is presented in Figure 12.

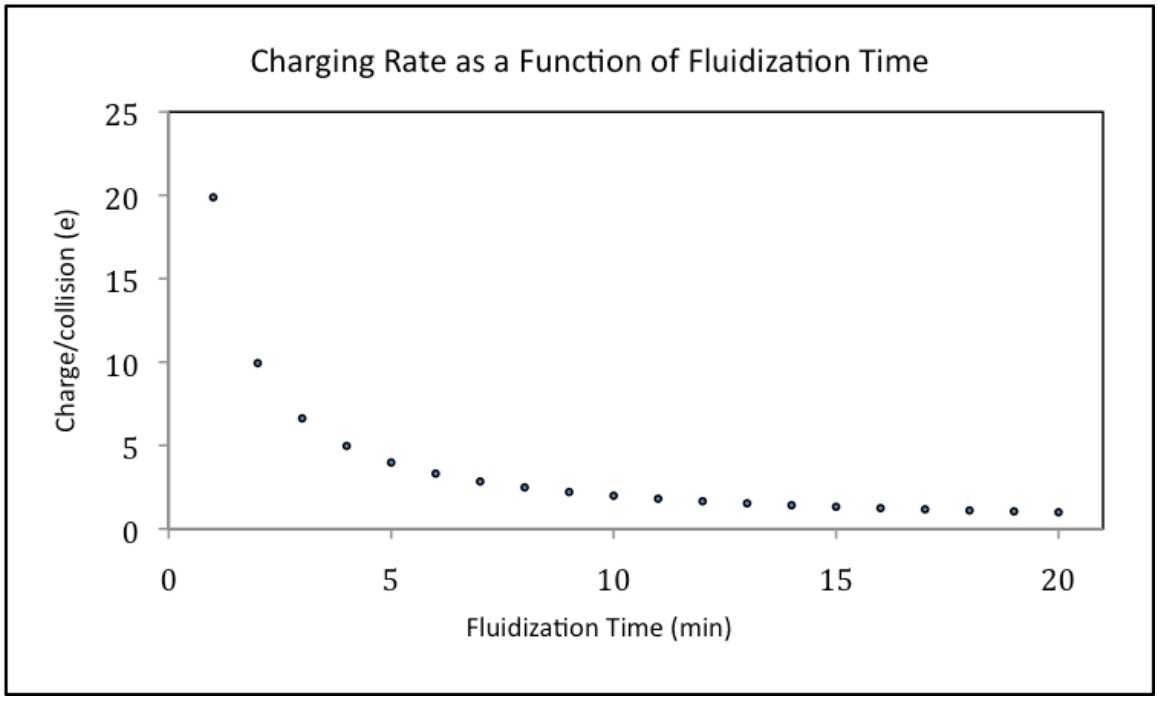

Figure 12: Charging rate as a function of fluidization time. The more time is assumed over which the charging occurs, the closer the value approaches our calculated value of 1.28 (±0.23) electrons transferred per collision.

As can be seen, short charging timescales introduce a significant variability in the final charge exchange rate. As larger and larger timescales are assumed, this value approaches a steady value; further applications of this work could include a more

thorough analysis of how the charge evolves over time. Figure 13 shows preliminary results at looking at *mass* of ash collected over time, though at the moment these results are somewhat out of context without data for longer timescales.

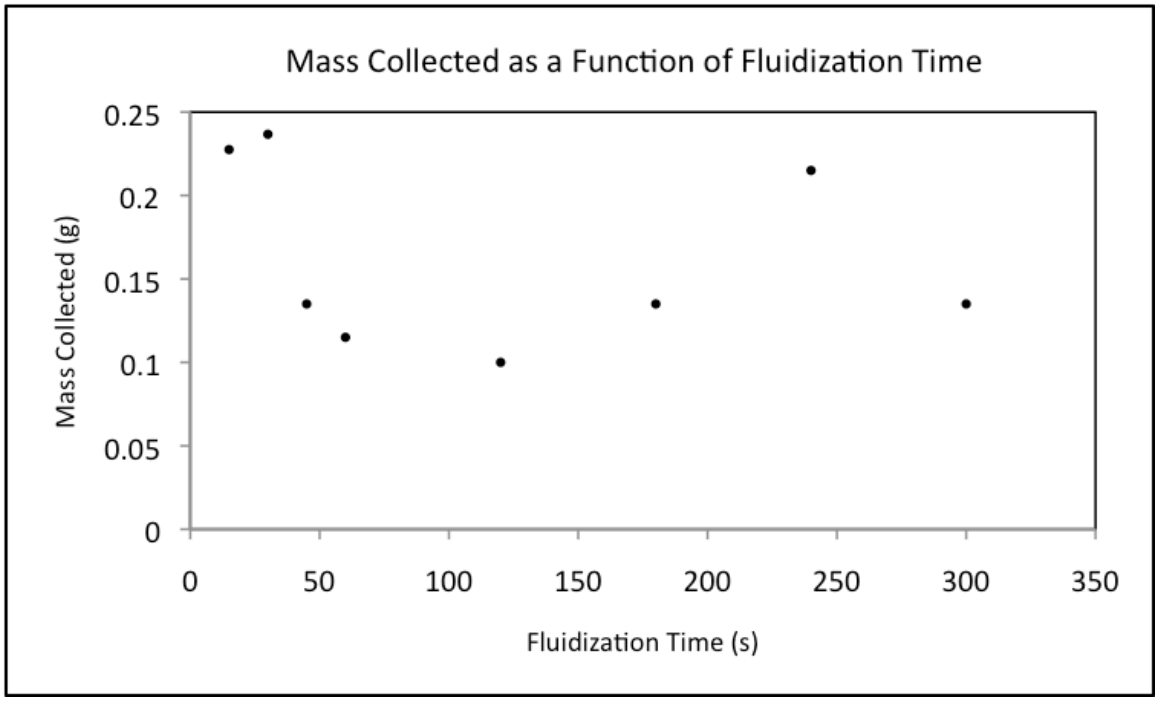

Figure 13: Mass of ash collected as a function of fluidization time. Note the spread in values, currently showing no distinct relationship between the two (very important to now that the data currently only extends to 350 seconds).

Figure 14 shows error calculations done examining possible variations in collection plate height, due to the configuration of the plate and bed and the possibility of errors made in measuring the plate height before each trial. As can be seen, if the recorded collection height is as much as 0.5 mm off of the actual value, this can skew the minimum charge by as much as 46%. This is why multiple height trials were performed, as well as rigorous methods to find the collection height as carefully as possible.

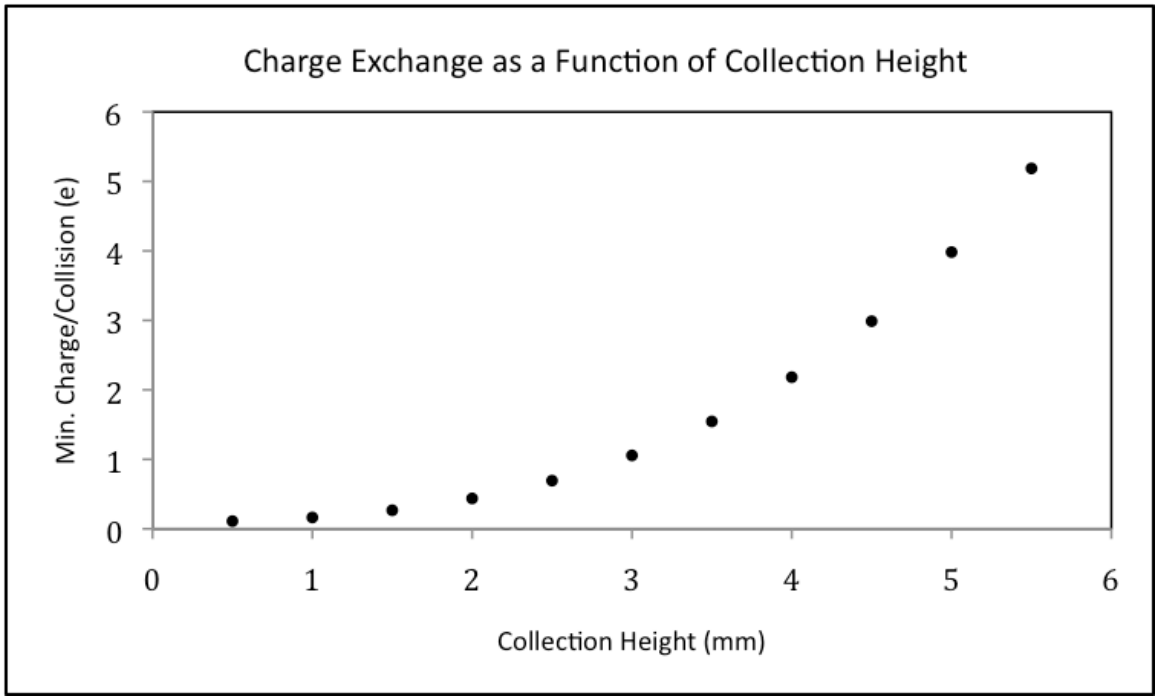

Figure 14: Charge exchange as a function of plate height. Note that even slight errors in the assumption of plate heights lead to large discrepancies in the minimum charge exchange calculation.

CHAPTER 5

FUTURE DIRECTIONS

Experimental Applications

This work represents the first application of the aforementioned principles to volcanic ash. Using lab techniques developed over the course of this thesis, a charge exchange rate, with constraints, was determined for the given configuration (see Figure 2). The next step for this work would be to expand on the data sets by replicating the experiments with different size 'bins,' ash from other volcanic locations, etc. This would validate the conclusions drawn here as to the correlation between size and associated polarity in collisional ash situations. The next experimental step from here would be to obtain better constraints on the timescales over which charging occurs. Though some work has been done in this thesis to address this issue (see Figures 12, 13), further experiments could yield more accurate timescales over which particles obtain, transfer, and discharge electrons. Once a more accurate measurement of the charging timescale has been made, further experiments on charging could be conducted, incorporating atmospheric conditions such as varying humidity and temperature; this would allow for a more accurate reflection of actual volcanic plume dynamics, rather than the dry ash experiments conducted here.

Numerical Applications

Developing better and more thorough constraints on the charge exchange in collisional ash flows would allow for the incorporation of charge dynamics into larger flow models. These models (*Dufek et al. 2007*) use Eulerian-Eulerian-Lagrangian methods to incorporate microscale and macroscale interactions within a convecting volcanic plume. The addition of charging mechanisms to these types of models would allow for a more complete picture of the dynamics affecting the motion and size of the volcanic plume.

APPENDIX A

RAW DATA

Table 2: Raw Data for experiments conducted.

Positive Data Image Name (IMG_####.jpg)	**Negative Data Image Name (IMG_####.jpg)**	**Data Files (+) (.txt)**	**Data Files (-) (.txt)**	**Corresponding Histogram**
1108-1111	1104-1107	5Dec2mmPos	5Dec2mmNeg	Figures 6,7
1112-1121	1122-1126	6Dec2mmPos	6Dec2mmNeg	n/a
1049-1043	1044-1053	30NovPos	30NovNeg	Figures 6,8
1054-1060	1061-1064	3DecPos	3DecNeg	n/a
1066-1070	1071-1074	3DecPos	3DecNeg	n/a
1084-1091	1080-1083	4DecPos4mm	4DecNeg4mm	n/a
1028-1033	1024-1027	hist_dataCpos	hist_dataCneg2	Figures 6,9
1075-1078	1079	4DecPos5mm	4DecNeg5mm	n/a
1095-1097	1098-1102	5DecPos	5DecNeg	Figures 6,10

REFERENCES

Anderson, R., Bjornsso.S, et al. (1965). "ELECTRICITY IN VOLCANIC CLOUDS - INVESTIGATIONS SHOW THAT LIGHTNING CAN RESULT FROM CHARGE-SEPARATION PROCESSES IN A VOLCANIC CRATER." Science **148**(3674): 1179-&.

Beitler, Jane (2009). "Experiment in the Sky." Nasa Research Article. 11 November 2009. http://nasadaacs.eos.nasa.gov/articles/2009/2009_volcanoes.html

Chakraborty, P., G. Gioia, et al. (2009). "Volcanic mesocyclones." Nature **458**(7237): 497-500.

Dufek, J. and G. W. Bergantz (2007). "Dynamics and deposits generated by the Kos Plateau Tuff eruption: Controls of basal particle loss on pyroclastic flow transport." Geochemistry Geophysics Geosystems **8**

Duff, N. and D. J. Lacks (2008). "Particle dynamics simulations of triboelectric charging in granular insulator systems." Journal of Electrostatics **66**(1-2): 51-57.

Dwyer, J. R., M. A. Uman, et al. (2009). "Remote measurements of thundercloud electrostatic fields." Journal of Geophysical Research-Atmospheres **114**.

Farrell, W. M., G. T. Delory, et al. (2003). "A simple electrodynamic model of a dust devil." Geophysical Research Letters **30**(20).

Farrell, W. M., N. Renno, et al. (2006). "Integration of electrostatic and fluid dynamics within a dust devil." Journal of Geophysical Research-Planets **111**(E1).

Forward, K. M., D. J. Lacks, et al. (2009). "Charge Segregation Depends on Particle Size in Triboelectrically Charged Granular Materials." Physical Review Letters **102**(2).

Hoblitt, R. P. (1994). "AN EXPERIMENT TO DETECT AND LOCATE LIGHTNING ASSOCIATED WITH ERUPTIONS OF REDOUBT VOLCANO." Journal of Volcanology and Geothermal Research **62**(1-4): 499-517.

James, M.R., Lane, S.J. and Gilbert, J.S. (1998) Volcanic plume monitoring using atmospheric electric potential gradients. *J*. *Geol*. *Soc*. *Lond*., **155**, 587-590.

James, M. R., L. Wilson, et al. (2008). "Electrical charging of volcanic plumes." Space Science Reviews **137**(1-4): 399-418.

Lacks, D. J., N. Duff, et al. (2008). "Nonequilibrium accumulation of surface species and triboelectric charging in single component particulate systems." Physical Review Letters **100**(18).

Lacks, D. J. and A. Levandovsky (2007). "Effect of particle size distribution on the polarity of triboelectric charging in granular insulator systems." Journal of Electrostatics **65**(2): 107-112.

Lamoreaux, P. E. (1995). "WORLDWIDE ENVIRONMENTAL IMPACTS FROM THE ERUPTION OF THERA." Environmental Geology **26**(3): 172-181.

Lowell, J. (1986). "CONSTRAINTS ON CONTACT CHARGING OF INSULATORS .1. SPATIAL LOCALIZATION OF INSULATOR STATES." Journal of Physics D-Applied Physics **19**(1): 95-104.

Manga, M., A. Patel, and J. Dufek, Rounding of pumice clasts during transport: field measurements and laboratory studies, *Bulletin of Volcanology*, **in press**

Pahtz, T., H. J. Herrmann, et al. (2010). "Why do particle clouds generate electric charges?" Nat Phys **6**(5): 364-368.

Parker, G. W. (2002). "Electric field outside a parallel plate capacitor." American Journal of Physics **70**(5): 502-507.

Shipley, S., Sarna-Wojcicki, A.M., 1982. Distribution, thickness, and mass of Late Pleistocene and Holocene tephra from major volcanoes in the northwestern United States: a preliminary assessment of hazards from volcanic ejecta to Nuclear reactors in the Pacific Northwest: U.S. Geological Survey Miscellaneous Field Studies Map. **MF-1435.**

Rasmussen, K. R., J. F. Kok, et al. (2009). "Enhancement in wind-driven sand transport by electric fields." Planetary and Space Science **57**(7): 804-808.

Riousset, J. A., V. P. Pasko, et al. (2007). "Three-dimensional fractal modeling of intracloud lightning discharge in a New Mexico thunderstorm and comparison with lightning mapping observations." Journal of Geophysical Research-Atmospheres **112**(D15).

Telling, J, Dufek, J (2010). "An experimental evaluation of the role of water vapor and collisional energy on ash aggregation in explosive volcanic eruptions." M.S. Thesis, Georgia Inst. of Technology.

Textor, C., H. F. Graf, et al. (2006). "Volcanic particle aggregation in explosive eruption columns. Part I: Parameterization of the microphysics of hydrometeors and ash." Journal of Volcanology and Geothermal Research **150**(4): 359-377.